RSC Advances

PAPER

View Article Online
View Journal | View Issue

Cite this: *RSC Adv.*, 2024, **14**, 9763

Hydrogen storage efficiency of Fe doped carbon nanotubes: molecular simulation study†

Bita Baghai[a] and Sepideh Ketabi *[b]

Given that adsorption is widely regarded as a favorable technique for hydrogen storage, it is appropriate to pursue the development of suitable adsorbent materials for industrial storage. This study aimed to assess the potential of Fe-doped carbon nanotubes (FeCNT) as a remarkable material for hydrogen storage. The structures of pure and Fe-doped CNTs were optimized based on quantum mechanical calculations using density functional theory (DFT) with the Perdew–Burke–Ernzerhof (PBE) method. To gain a comprehensive understanding of the adsorption behavior, Monte Carlo simulation was employed to investigate the adsorption of hydrogen molecules on FeCNT. The study specifically examined the impact of temperature, pressure, and hydrogen mole percentage on the adsorption capacity of FeCNT. The findings indicated that the uptake of hydrogen increased as the pressure increased, and when the pressure exceeded 5 MPa, FeCNT reached a state of near saturation. At room temperature and pressures of 1 and 5 MPa, the hydrogen capacities of FeCNT were determined to be 1.53 and 6.92 wt%, respectively. The radial distribution function diagrams confirmed the formation of a one-layer adsorption phase at pressures below 5 MPa. A comparison of the temperature dependence of hydrogen adsorption between FeCNT and pure CNT confirmed the effectiveness of Fe doping in hydrogen storage up to room temperature. FeCNT exhibited a greater reduction in initial hydrogen capacity at temperatures above room temperature. To evaluate the safety of the system, the use of N_2 as a dilution agent was investigated by examining the hydrogen uptake of FeCNT from pure and H_2/N_2 mixtures at 300 K. The results showed that the addition of N_2 to the environment had no significant effect on FeCNT hydrogen storage at pressures below 4 MPa. Furthermore, the study of H_2 selectivity from the H_2/N_2 mixture indicated that FeCNT demonstrated a preference for adsorbing H_2 over a wide range of bulk mole fractions at pressures of 4 and 5 MPa, suggesting that these pressures could be considered optimal. Under these conditions, Fe doping can offer an efficient and selective adsorption surface for hydrogen storage.

Received 8th December 2023
Accepted 18th March 2024

DOI: 10.1039/d3ra08382a

rsc.li/rsc-advances

1. Introduction

Due to excessive consumption of non-renewable energy sources such as fossil fuels in the past few decades, this energy source is expected to end abruptly. Since fossil fuels cause excessive emission of greenhouse gases, they have a large contribution to the problem of global warming and climate change.[1] Therefore, due to these problems and the reduction of non-renewable energy reserves, it is necessary to improve new technologies for renewable energy sources. One of the newest renewable energy sources is the technology based on hydrogen energy.

Hydrogen is a useful clean energy carrier and has attracted much attention in science and technology.[2] Therefore, an effective, safe, and inexpensive system with high hydrogen storage capacity, at temperatures from ambient to 100 °C and pressures below 100 bar is fundamental in practical applications.[3–6] To achieve these conditions, it is better to use the interaction of hydrogen with solids instead of compressed or liquid hydrogen (which needs high pressures or low temperatures).[2,6]

Suitable experimental and theoretical investigations have been stated to attain extremely effective hydrogen storage materials, containing several nanotubes,[7] metals, and organic functional groups.[8] The hydrogen storage ability of carbon nanotubes (CNTs) is a vital research topic that has attracted worldwide attention.[9]

Among several potential solid adsorbents, CNTs, which are one-dimensional tubular carbon allotropes, were considered due to their significant surface area, porous structure, and tremendous thermal and chemical stability.[10] CNTs, originally

[a]Department of Applied Chemistry, Faculty of Pharmaceutical Chemistry, Tehran Medical Sciences, Islamic Azad University, Tehran, Iran

[b]Department of Chemistry, Faculty of Pharmaceutical Chemistry, Tehran Medical Sciences, Islamic Azad University, Tehran, Iran. E-mail: sepidehketabi@yahoo.com; s.ketabi@iautmu.ac.ir

† Electronic supplementary information (ESI) available. See DOI: https://doi.org/10.1039/d3ra08382a

developed and reported by S. Iijima,[11] are made of rolled graphene sheets.[12] Due to their unique structural, electronic, and mechanical properties, CNTs have significant potential in chemical and biological applications.[13] Since CNTs have substantial physical and chemical properties, they have numerous applications in nanoelectronic devices and optoelectronics,[14] FETs, LEDs,[15] polymer composites,[16,17] chemical sensors and biosensors,[18,19] *etc.*

The famous properties of CNTs related to binding with hydrogen molecules have proven their good adsorption properties in environmental conditions.

Despite the ability of CNTs in hydrogen energy storage, they are reported to show very low hydrogen uptake capacities,[20] which is due to their weak van der Waals interaction with hydrogen.[21]

Several approaches have been applied to improve low hydrogen adsorption of CNTs. One of the effective methods in this context is doping with other atoms,[22,23] which induces defects in the nanotubes. Doping is an approach used to modify the properties of materials and involves introducing impurities or foreign atoms into a material to alter its properties. This technique can be utilized to enhance conductivity, modify band gaps, or induce magnetic properties.[24,25]

By introducing heteroatoms into the structure of nanotubes, the doping process can modify their properties, enhance their functionality, and induce defects in their structure.

Defects play a significant role in determining the properties and applications of materials. They range from doping in semiconductors to conductivity in mixed ionic–electronic conductors used in batteries, as well as active sites in catalysts.[26–28] The disruption of translational symmetry at a defect site induces changes in the local degrees of freedom, which can be classified into configurational, vibrational, spin, and electronic terms. Metal doping affects the structure of carbon nanotubes by introducing changes in their morphological characteristics, compositions, and surface functionality. When doping nanotubes, impurities can be intercalated inside a nanotube, in the space between separate nanotubes, or can substitute one of the atoms of a nanotube. This localization of impurities within the nanotube or between separate nanotubes reduces the likelihood of their migration.

Previous research has also reported the enhancement of H_2 absorption and storage in Vanadium oxide nanotube (VONT) by doping some transition metals.[23,29] Experimental studies have shown that chemical functionalization and metal doping can improve the hydrogen adsorption capacity of CNTs.[30] Defects on the CNT surface have induced the caps to open and thus increase the active sites for the adsorption of hydrogen molecules.[31]

During the synthesis of CNTs, different factors affect the hydrogen adsorption capacity of CNTs such as synthesis conditions, impurity, and catalyst substances. The metal contaminations in CNT can affect the storage capacity.[32] It has been shown that transition metal loading to the carbon structure could improve hydrogen uptake[33] of the carbon structures.[34] Changes of CNT structures by transition metal doping[35–38] and transition metal oxide nanoparticle[39–42] have been also reported to enhance H_2 adsorption capacity. Numerous studies have demonstrated that the addition of metals such as Ni, Pd, Fe, Pt, Co, and V to carbon structures enhances their hydrogen storage capacity.[26,38,39,43–46] Doping carbon nanotubes with Ti at different locations enhances their structural stability, thermodynamic parameters, and hydrogen adsorption.[33] Experimental evidence has shown that CNTs grown on Fe, V, Co, and Ni catalysts exhibit H_2 adsorption capacities ranging from 2.76 to 5.25 wt%, with CNTs grown on Fe catalyst displaying the highest H_2 uptake.[47] Recent findings revealed that Fe/CNTs have a higher hydrogen storage capacity at room temperature compared to Co/CNTs.[46] Studies on the deposition of Al atoms on Fe-doped CNTs indicated that the Fermi level and energy gap of the CNTs decrease after doping with Fe atoms. Fe doping also disrupts the original electron transfer property of the CNTs, potentially leading to an enhanced interaction with gas molecules.[48] As a transition metal, Fe provides active sites that surpass those of C,[49] and can form stable chemical structures with a variety of reagents. Furthermore, Fe has a work function similar to that of CNTs, resulting in low contact resistance with CNTs.[50] Therefore, it can be concluded that Fe is a suitable metal dopant for modifying and improving the gas adsorption properties of CNTs.[51]

Moreover, it has indicated that the hydrogen storage of CNTs was influenced by the applied catalyst during the synthesis.[47] The CNTs that grow on Fe have shown maximum hydrogen storage capacities.

Recently, effect of Ti and N doping on the hydrogen adsorption abilities of two-dimensional carbon layers have been investigated.[52] The outcomes indicated that the hydrogen storage potentials of graphene nano layers can be improved by increasing the concentration of Ti atoms.

Ab initio molecular dynamics (AIMD) using the local density approximation has been employed to simulate the behavior of trimethyl indium $(CH_3)_3In$ (TMIn) on graphene supported by SiC in an H_2 atmosphere and on freestanding graphene. The purpose of this endeavor was to acquire knowledge about the reaction dynamics involved in the supply of In atoms to the graphene surface.[53] The focal point of the study was a model that encompassed the zero-layer graphene exposed to TMIn and hydrogen molecules. Through the simulations, the atomistic pathways for TMIn transformations were unveiled, ultimately resulting in the formation of isolated In or InH species on the graphene surface. In particular, it was observed that TMIn exhibited heightened reactivity in the presence of H_2, thus confirming the chemical affinity between In and hydrogen species.

In another recent study, Fe-doped carbon aerogels with different percentages of iron atoms were synthesized.[54] The results indicated that increasing Fe content induced a decrease in hydrogen adsorption. However, Fe-doped activated carbon aerogels showed enhanced hydrogen storage due to the formation of CNTs in the matrix.

Transition metal (Fe, Ni, and Cu) doping can affect the electrocatalytic activity of the M-Co_2P/NCNTs hybrid catalysts for hydrogen evolution reaction. The results have revealed that Fe doping resulting a large adsorption surface and active sites

due to the large surface area and greatest partial charge of Fe after doping.[55]

Os-doping and Fe-doping have been applied to enhance the effectiveness of (9,9) CNT for hydrogen adsorption.[56] Electron energy loss functions and the optical adsorption coefficients of the nanotubes have been computed by density functional theory (DFT) method and the result of metal doped CNTs have been compared with pristine CNT. It has been concluded that transition metal doping can increase the hydrogen adsorption ability of CNTs. An enhancement in adsorption efficiency was attained due to the doping of Fe and Os atoms, which overcomes the weak interactions between pristine CNT and hydrogen molecules. In this investigation, quantum mechanical calculations were utilized to compare the adsorption of two H_2 molecules on pure and metal-doped CNTs.[56] The efficacy of H_2 adsorption was examined by analyzing the interactions between light and the studied systems, accomplished by determining the complex dielectric functions. As stated, Fe doping of pristine CNTs enhanced the power efficiency of H_2 energy storage in single-walled CNTs. To assess the H_2 adsorption capacity of CNTs under different temperature and pressure conditions in an H_2 environment (where the number of H_2 molecules is proportional to the pressure and temperature), either experimental methods or molecular simulation calculations can be employed.

As previously mentioned, experimental studies on hydrogen adsorption of Fe-decorated CNTs have confirmed an improvement in the hydrogen adsorption of CNTs.[38] The hydrogen storage capability of the CNTs has been evaluated using volumetric and electrochemical techniques under ambient pressure. To determine the optimal conditions of temperature and pressure for hydrogen adsorption capacities, computer simulation methods were applied to these CNTs in our study. Particularly, the investigation focused on the hydrogen adsorption capacities from mixtures of gases, as the addition of N_2 to the system dilutes the hydrogen environment and enhances safety, which is more favorable for fuel cell applications. Our findings contribute to a better understanding of the fundamental principles and optimal conditions for H_2 storage in CNTs, thus shedding light on the rational design of nanoarchitectures for energy storage.

Due to the limitations of experimental conditions, simulation methods are often employed to elucidate microscopic information that cannot be obtained or observed through experiments. By analyzing the acquired information within a wide range that is not easily accessible in practical settings, theoretical calculations have been conducted to investigate the adsorption characteristics of the adsorbent.

The objective of the present research is to assess the impact of Fe doping on the H_2 adsorption of carbon nanotubes. Due to the challenges associated with experimentally characterizing the structure properties of the adsorbent, molecular simulation can be employed to determine the optimal adsorption conditions. Molecular simulation allows for the evaluation of selectivity and the relationship between the adsorption properties and the structure. Therefore, our study has organized various relevant variables to predict the optimal conditions for hydrogen storage.

Monte Carlo (MC) simulation method was implemented to compare the absorption capacity of Fe doped CNT (FeCNT) and pristine CNTs. Hydrogen uptake from both pure environments and mixtures of H_2 and N_2 in Fe-doped CNTs was anticipated. By evaluating the effects of temperature and pressure on the hydrogen adsorption of FeCNT and pristine CNTs, the optimal conditions for hydrogen storage were determined. The radial density profile of the adsorbed phase was evaluated. Additionally, the effects of bulk pressure and composition on hydrogen selectivity from gas mixtures were defined.

2. Computational details

2.1 Quantum mechanics

Optimization of pure and Fe doped CNTs was carried out by quantum mechanical calculations. (9,9) CNT with Fe doped at 20 wt% level was considered as an absorbent in hydrogen adsorption. FeCNT was obtained by replacing the C atom in the CNT structure. Characteristics of studied FeCNT were stoichiometry of $Fe_{14}C_{256}$, length of 18.51 Å, and a diameter of 14.15 Å.

Different percentages of Fe loading have been utilized in several studies. In a recent investigation, Fe7%-CNT has been employed to catalyze the oxygen reduction reaction.[57] Similarly, in another study, composites of multi-walled CNTs doped with 8 wt% Fe were extensively used to enhance the electromagnetic interference (EMI) shielding effectiveness (SE) of CNTs. The Fe concentrations in the composites were measured at 0.08 wt%.[58] Additionally, Fe-doped carbon aerogels were synthesized with Fe doping at different dopant levels of 1, 5, and 10%. These aerogels exhibited a hydrogen uptake of 3.8 wt%.[54] Consequently, considering the existence of prior studies on hydrogen absorption involving lower percentages of Fe doping, our focus was on investigating the synergistic and symmetrical effects surrounding the nanotube. To this end, we conducted hydrogen storage studies on a doped nanotube with a 5 mole percent Fe doping. In future investigations, the authors plan to employ varying metal percentages to elucidate the impact of Fe dopant percentage on the hydrogen storage properties of CNTs.

It is important to acknowledge that the stoichiometry of metal doped CNTs in actual experimental studies might differ from that of modeling studies. Nevertheless, these models should be taken into consideration of other experimental or computational evidence. Moreover, it should be noted that, like our research, doping has been employed in other studies as well.[51,56,59]

In one particular study, in order to achieve a notable doping effect, Os- or Fe-doped CNT models were obtained by replacing the C atoms in the CNT structure.[56] In the study of CO[59] and SO_2 (ref. 51) adsorption properties of Fe-doped CNTs, the same approach as in our current research was adopted. Fe–CNT was also constructed by replacing an intrinsic CNT with a Fe atom, and the adsorption energies were determined through quantum mechanical calculations.

In the case of such dopants, they constitute an inherent part of the matrix lattice, thereby resolving the issue of dopant

clustering. However, in other systems, this doping method may result in clustering or the formation of more intricate systems. This conclusion is illustrated by the storage of Li in graphene, where the separation of Li phases leads to significant capacity limitations.[60] Li loading results in a strong repulsion between Li ions at neighboring hexagons.[61] Additionally, the positive lithiation energy of graphene implies that the Li adatoms on it should aggregate into clusters and eventually form macroscopic dendrites, instead of forming any stable Li-graphene mixture phase. First-principles computations have shown that the doping of pristine graphene with Li can be stabilized by employing the layered C3B compound, which holds promise as a storage medium at defected adsorption sites. In the case of Li, since it donates its 2s electron to the matrix, an electron-deficient matrix, such as B-substituted C, can better accommodate the extra electrons. However, in the case of transition metals, due to the presence of electrons in the d orbitals, this issue is slightly different. The presence of empty d orbitals enables a direct and stable interaction with C, leading to the creation of defect sites in doping sites.[62] It was shown that the CNT doped with Ni resulting in electronic charge transfer and formation of Ni–C bonds at the interface between these two materials.[63] In the current study, we employed the generalized-gradient approximation (GGA) with the Perdew–Burke–Ernzerhof (PBE) method as the exchange–correlation functional.[64,65] To achieve a balance between computational effort and accuracy, the Brillouin zone sampling, $1 \times 1 \times 3$ Monkhorst–Pack mesh was used for the k-point summation. Spin-unrestricted DFT calculations were accomplished for (9,9) CNT and FeCNT. The QUANTUM ESPRESSO package[66] was utilized for computations. In the next simulation step, optimized geometries were employed.

2.2 Monte Carlo simulation

Due to the limitation of experimental conditions, simulation methods are usually used for determining microscopic information that cannot be obtained or observed in experiments. By analyzing the adsorption capacities, distribution of gas molecules, selectivity, and other information in a wide range that is not easily accessible in practice, theoretical calculations have been performed to study the adsorption characteristics of adsorbent. To explore the adsorption of H_2 molecules in FeCNT, MC simulations were employed at the pressures 0.1–10 MPa and temperatures 75–350 K.

The MC simulations were accomplished in a cubic box with the size of 50 Å at the experimental pressures and temperatures applying the Metropolis sampling algorithm.[67] The alignment of the nanotube was placed along the z-axis. The Virial equation of state with second and third coefficients was applied to compute gas molecule densities at the studied temperatures and pressures.[68] Compression factor (Z) as a function of temperature and pressure is illustrated in the following formula:[68]

$$\frac{P}{\rho RT} = Z = 1 + B_{\text{mix}}\rho + C_{\text{mix}}\rho^2 \quad (1)$$

where, ρ is density, B_{mix}, and C_{mix} are the mixture second and third Virial coefficients, which are functions of temperature and composition. B_{mix} and C_{mix} are represented as below:

$$B_{\text{mix}} = \sum_i \sum_j x_i x_j B_{ij} \quad (2)$$

$$C_{\text{mix}} = \sum_i \sum_j \sum_k x_i x_j x_k C_{ijk} \quad (3)$$

x_i, x_j and x_k are the mole fractions of the ith, jth and kth components of the mixture. B_{ij} and C_{ijk} are cross second and third Virial coefficients which are given by:

$$B_{\text{mix}} = b_{ij,0} + \frac{b_{ij,1}}{T} + \frac{b_{ij,2}}{T^2} \quad (4)$$

$$C_{\text{mix}} = c_{ijk,0} + \frac{c_{ijk,1}}{T} + \frac{c_{ijk,2}}{T^2} \quad (5)$$

The appropriate coefficients were applied in eqn (4) and (5).[68,69]

New configurations were created by randomly selecting a molecule and translating it in three dimensions. Periodic boundary conditions were employed in three dimensions.

A reasonable range of translations has been used to achieve a 50% acceptance rate for the produced configurations.

The required configurations of the system were established to calculate the equilibrium properties. Each point is the result of 10^8 attempts to move. One molecule was picked and displaced randomly in three dimensions x, y, and z. An acceptance rate of 50% for new configurations was achieved by using suitable ranges for translations. The central axis of the nanotube is located along the z-axis.

The initial 5×10^7 cycles were applied for equilibrium and the second 5×10^7 cycles were used to verify ensemble averages. Periodic boundary conditions were applied in all three dimensions and a reflection plane.

The interactions of atoms included bonding parts (between chemically bonded atoms) and non-bonding parts (between any pair of atoms). To calculate the non-bonding interaction energies between the gas–CNT and gas–gas, Lennard-Jones potential function was applied:

$$E_{ij}^{\text{AB}} = 4\varepsilon_{ij}\left[\left(\frac{\sigma_{ij}}{r_{ij}}^{12} - \left(\frac{\sigma_{ij}}{r_{ij}}\right)^6\right)\right] \quad (6)$$

where, σ_{ij} and ε_{ij} are Lennard-Jones (LJ) size and energy parameters, respectively. Suitable Lennard-Jones parameters for carbon atoms in CNT[70] and Fe[71] were implemented in calculations. H_2 and N_2 were characterized as spherical molecules with effective size and energy parameters.[72–74] The total interaction energy between gas molecules and each site of CNT is expressed by the pair-wise sum of their interaction contributions:

$$E_{\text{ab}} = \sum_i^{\text{ona}} \sum_j^{\text{onb}} E_{ij}^{\text{AB}} \quad (7)$$

The site–site Lennard-Jones parameters ε_{ij} and σ_{ij} for the cross-interaction were obtained according to Lorenz–Berthelot (LB) combining rule[75] (the interacting sites i and j are from different species):

$$\sigma_{ij} = \frac{1}{2}(\sigma_i + \sigma_j) \quad (8)$$

$$\varepsilon_{ij} = (\varepsilon_i \varepsilon_j)^{\frac{1}{2}} \quad (9)$$

Lennard-Jones cross-interaction parameters are indicated in Table 1.

The Lennard-Jones potential between each pair falls off very rapidly with distance and at 2.5σ the intermolecular interactions have just 1% of its value at σ.[76] Therefore, A spherical cut-off distance of 7.5 Å was deployed to the potential interactions between hydrogen molecules.

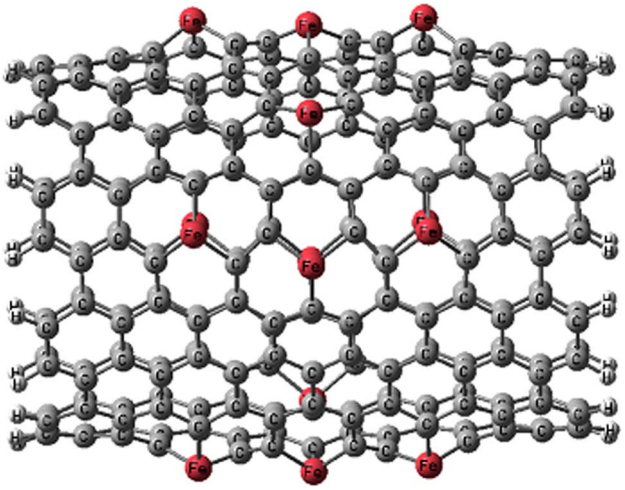

Fig. 1 Optimized structure of FeCNT.

3. Results and discussion

3.1 Quantum mechanics

After full structural optimizations, Fe-doping causes significantly large distortion in CNT (Fig. 1). Fe atoms move towards the outside of the tube diameter and visible local geometric distortion occurs around the Fe atoms after substituting the Fe atom for the C atom. This is mainly attributed to the difference between the atomic radius of Fe and C. The average Fe–C bond lengths in FeCNT are 1.96 Å, which are significantly larger than the C–C bonds (1.420 Å) of pristine CNT. The increase in the bond lengths combined with the difference in bond angles forces the Fe atoms to protrude outwardly from the nanotube surface.

The formation energy for Fe-doping into the CNT was defined as

$$E_F = (E_{FeCNT} - E_{CNT}) - n \times (E_{Fe} - E_C) \quad (10)$$

where E_{FeCNT} is the total energy of CNTs with substitutional doping, E_{CNT} is the total energy of pristine CNTs, E_{Fe} is the energy of a single free doping atom, E_C is the energy of a single free carbon atom, and n is the number of doping atoms (14 in the current study).[77,78] The formation energy is dependent on the radius and chirality of the nanotube.[77–81] The calculated formation energy of Fe-doped CNT was 21.34 eV. Our results are comparable with earlier calculated formation energies of metal doped CNTs. In the study of the effect of transition metal (Fe, Co, or Ni) doping on the adsorption properties of (10,10) CNT, an assessment has been conducted on the formation energy of metal doping.[78] The findings have demonstrated that the formation energies for replacing one and two carbon atoms with Fe in CNT are 8.59 and 14.59 eV, respectively. In the study of Si-doping in CNTs[77] the calculated energy of forming Si-doped (5,5) CNT has been obtained at about 7.142 eV. Moreover, it has been stated that the double substituted CNT is easier to form than that of one Si atom (the formation energy was 12.594 eV). Moreover, the density functional study of geometric and electronic structures of Eu-doped CNT indicated that the formation energy of Eu substituting for one carbon atom in CNT (6,6) is 2.53 eV. In another study,[81] a single Fe atom is used to substitute one Si atom or C atom in a SiC nanotube with a formation energy of 6.26 and 9.46 eV, respectively. In their structure, the Fe atom moves towards the outside of the tube wall and forms a triangular pyramidal tetrahedron structure. According to the formation energy results, it has been anticipated that the Fe atom is more inclined to replace the Si atom. This is primarily due to the significantly larger atomic radius of Fe compared to that of C, resulting in a reduction in the local symmetry surrounding the Fe atom and the stability of bonds. However, the two types did not change the original structure of SiC nanotube, thus rendering them stable in the presence of Fe.

Table 1 Lennard-Jones cross-interaction parameters

Cross interaction	ε_{ij} (kcal mol^{-1})	σ_{ij} (Å)
H_2–Fe	0.8210	2.640
H_2–C	0.0764	3.230
N_2–Fe	0.8160	2.820
N_2–C	0.0759	3.410

3.2 Monte Carlo simulation

It has been verified that metal doping can modify the electronic structure, adsorption properties, and activity of surfaces.[82] To evaluate the effect of Fe doping on the adsorption properties of CNT, H_2 adsorption capacity and the adsorption isotherms of FeCNT were determined by the Monte Carlo simulation method.

To evaluate nanotube gas uptake, the adsorption capacity can be an important consideration. Gas adsorption can be assessed in terms of gravimetric adsorption capacity at different temperatures and pressures.

The gravimetric adsorption capacity of pure gases in a nanotube (ρ_w or wt) is determined by the following equation:[83,84]

$$\rho_w(\text{gas}(i)) = \frac{N_{\text{gas}(i)} M_{\text{gas}(i)}}{N_{\text{gas}(i)} M_{\text{gas}(i)} + M_{\text{NT}}} \quad (11)$$

where $M_{\text{gas}(i)}$ and M_{NT} denote the molar mass of gas and nanotube, respectively; $N_{\text{gas}(i)}$ denotes the number of adsorbed gas molecules; and i denotes H_2 in this study.

The gravimetric gas (i) adsorption capacity from a mixture of gases are determined by the following equation:

$$\rho_w(\text{gas}(i)) = \frac{N_{\text{gas}(i)} M_{\text{gas}(i)}}{N_{\text{gas}(i)} M_{\text{gas}(i)} + M_{\text{NT}} + \sum N_{\text{gas}(j)} M_{\text{gas}(j)}}. \quad (12)$$

where j represents other gases in the environment. i and j are H_2 and N_2 in this study.

Adsorption capacities of FeCNT from pure and mixture of H_2/N_2 were determined in different temperatures and pressures. The outcomes have been described in percent adsorption capacity (wt%).

3.2.1 Pure H_2 adsorption: adsorption isotherms. To assess the equilibrium occurrence of the uptake processes, the adsorption isotherms were implemented to develop the adsorption outcomes. The isotherms provide a graphical representation of the relationship between the amount of adsorbed phase and the gas phase. Furthermore, the isotherms depict the distribution of adsorbable gas between the adsorbent and the gas phase under equilibrium conditions. Considering the significant influence of temperature and pressure on the adsorption process, the optimal conditions for hydrogen adsorption on FeCNT were investigated.

The H_2 adsorption of FeCNT was calculated up to 10 MPa at different temperatures. Fig. 2 compares the gravimetric adsorption isotherms of H_2 on FeCNT under different pressures within the temperature range of 175–350 K. As can be seen, hydrogen adsorption capacity is a function of the pressure and temperature. At lower pressures, hydrogen uptakes are similar at different temperatures. As anticipated, hydrogen adsorption capacities reduced with increasing temperature, while an increase in adsorptions was observed followed by a pressure increase. As the pressure increases, the FeCNT can adsorb significantly higher amounts of H_2. At 175 and 200 K, and pressures larger than 5 MPa, hydrogen capacity decreases (and becomes constant) due to the high gas density in low temperatures and high pressures which produce a saturated phase. As the bulk pressure increases, adsorption (at low temperatures) is not favorable due to the endothermic process (which leads to particle–particle repulsion) and entropy reduction. Hence, a reduction in adsorption capacity is observed.

Hydrogen adsorption isotherms inside and outside the FeCNT are indicated in Fig. 2. It can be seen that the isotherms exhibit similar trends. Nonetheless, due to the steric restriction, hydrogen adsorption inside the FeCNT was lower than outside.

Fig. 3 presents the total capacity for H_2 sorption at different pressures and three temperatures. As observed, at pressures greater than 5 MPa, FeCNT is nearly saturated at all three temperatures, with a maximum adsorption capacity of about 9%. To determine the exact H_2 storage of FeCNT, the total H_2 uptakes at different pressures and temperatures are tabulated in Table 2.

As can be seen, of all reported temperatures, the highest amount of H_2 uptake by FeCNT falls within the range of 9–10%. The adsorption values at 10 MPa and, 175, 250 and 298 K were 10.086%, 9.4369%, and 9.1130% respectively. Therefore, it can be concluded that FeCNT can enhance the hydrogen adsorption potential of CNTs and exceed the target of the United States Department of Energy (DOE) (6.5 wt%).[85,86]

Many researchers have investigated the doping effect on the hydrogen adsorption of nanotubes. It has revealed that hydrogen storage of CNT and B doped CNT was 0.02 and

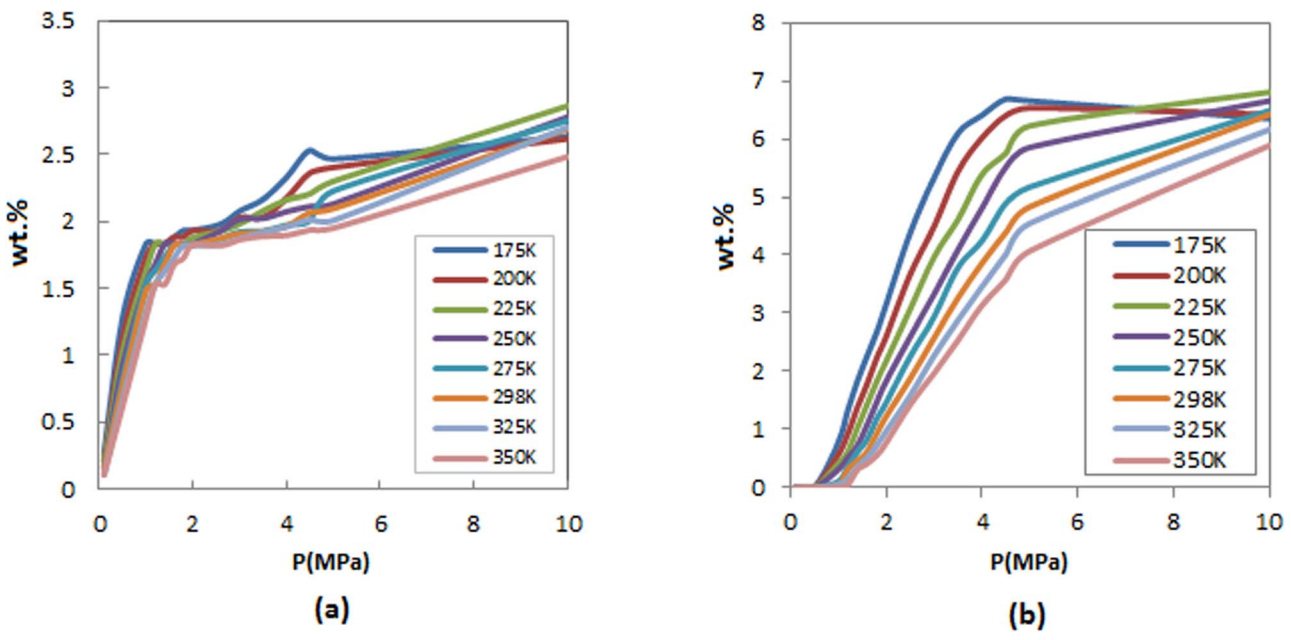

Fig. 2 Comparison of H_2 adsorption isotherms of FeCNT (a) inside (b) outside the nanotubes at different temperatures.

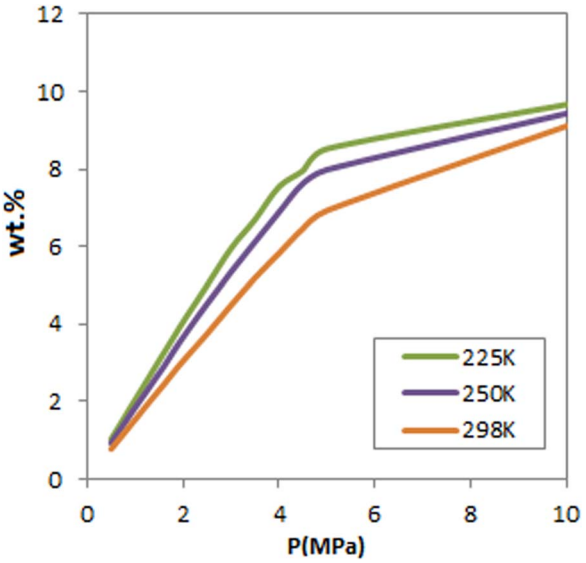

Fig. 3 Total H_2 adsorption isotherms of FeCNT at 225, 250 and 298 K.

Table 2 Total adsorption capacity of FeCNT at selected temperatures

P (MPa)	Total wt% 75 K	175 K	250 K	298 K
0.1	0.5673	0.2587	0.1554	0.1554
0.5	2.9280	1.2801	0.9250	0.7720
1	5.5341	2.6040	1.8417	1.5323
2	9.4252	5.0890	3.6632	3.0504
4.5	10.1821	9.2211	7.6277	6.4612
5	10.2993	9.1235	7.9834	6.9294
10	10.0417	10.0861	9.4369	9.1130

0.157 wt% at 303 K and 10 bar.[87] Volumetric measurements of H_2 storage of Pd and V doped CNT have confirmed the enhancement of the adsorption capacity of CNTs upon metal doping.[39] The results have indicated that H_2 uptake of Pd and V doped CNT at 298 K and 65 bar have been 0.125 and 0.1% respectively which were higher than hydrogen storage of CNT (<0.01%). Their results are comparable with our outcome of FeCNT adsorption capacity at 298 K and 0.5 MPa which was 0.77%. The higher H_2 adsorption capacity of FeCNT concerning V doped CNT and pure CNT can be also attributed to the ε_{ij} values of H_2–V,[29] H_2–Fe, and H_2–C (see Table 1). DFT investigations[88] have also revealed that the enhancement of hydrogen storage by metal doping is due to the electron transfer from metal atoms to carbon.

Many other studies have shown that hydrogen adsorption capacity is increased by metal doping.[89–95] The hydrogen adsorptions of the multi-wall CNT and Fe-multi-wall CNT which have been studied by volumetric and electrochemical methods in environmental conditions, were determined to be 0.3% and 0.75%, respectively.[38] The results revealed that H_2 molecules are adsorbed on the defect sites and pass into the spaces between neighboring carbon layers. The outcomes are compatible with our foundation at 298 K (Table 2), the differences are due to the single wall nanotube applied in the current study. In a recent study, Fe-doped carbon aerogels have been applied for hydrogen uptake at 77 K at pressures up to 30 atm.[54] Hydrogen adsorption capacities for 1, 5, and 10% Fe doped carbon aerogels at 25 atm and 77 K were 1.47, 1.38, and 1.28 wt%, respectively. Although the adsorption properties of Fe doped carbon aerogels are different from FeCNT, the results can be comparable with our outcomes. As can be seen in Table 2, FeCNT could adsorb 9.4252 wt% of H_2 at 2 MPa and 77 K and was almost saturated at larger pressures.

One of the objectives of the present study is to compare the hydrogen adsorption of FeCNT and pure CNT, and to confirm the efficiency of Fe doping in hydrogen storage of CNTs. Fig. 4 presents a comparison of the H_2 adsorption isotherms of FeCNT and pure CNT as a function of pressure at three different temperatures: 170 K, 250 K, and 298 K. At lower pressures, both nanotubes exhibit similar storage capacities. However, as the pressure increases (specifically, pressures exceeding 4.5 MPa), the hydrogen storage of FeCNT surpasses that of pure CNT. Comparison of the H_2 adsorption capacities of CNT and FeCNT can also be seen in Table S1.† These findings indicate that at pressures below 4 MPa, the Fe doping did not have a significant impact on the hydrogen adsorption of CNT, as evidenced by Fig. 4. However, at higher pressures, there is a slight improvement in H_2 adsorption with FeCNT. Nevertheless, under certain conditions, there are notable changes in the adsorption capacities of FeCNT. For example, at 4.5 MPa and 175 K, the H_2 adsorption of CNT and FeCNT were 8.0780% and 9.2211% respectively, representing an approximately 14% increase in adsorption. Similarly, at 5 MPa and 250 K, a 7% improvement was observed, and at 10 MPa and 250 K, a 17% enhancement in H_2 storage was observed due to Fe doping of CNT. However, one advantage of Fe doping on the hydrogen storage performance of CNT is the improved H_2 selectivity from an H_2/N_2 mixture environment, which will be discussed in Section 3.2.6. These findings reveal that the H_2 storage behaviors of CNT and FeCNT are comparable across all three temperatures but are enhanced by Fe doping at pressures above 4.5 MPa. Consequently, Fe-doping of CNT can be considered a viable strategy for achieving efficient H_2 storage at elevated pressures.

The highest hydrogen adsorption capacity that could be obtained for pure CNT was 4.84 wt% at 10 MPa and 77 K,[96] which has been determined by the volumetric method. By acid treatment of CNTs and removal of metal catalysts, a higher storage capacity of CNTs has been observed. The reason was that acid treatment damages the structure of CNTs, and as a result, structural defects with high energy sites can enhance hydrogen adsorption. Our results for FeCNT showed that the H_2 adsorption capacity is higher than pure CNTs.

A recent investigation that confirms the effectiveness of transition metal doping on the hydrogen uptake of CNTs has applied optical adsorption spectra analysis in the framework of DFT calculations.[56] As mentioned earlier, Fe and Os doping have been shown to overpower the weak interactions between CNT and hydrogen, thus affording a strong surface for hydrogen adsorption.

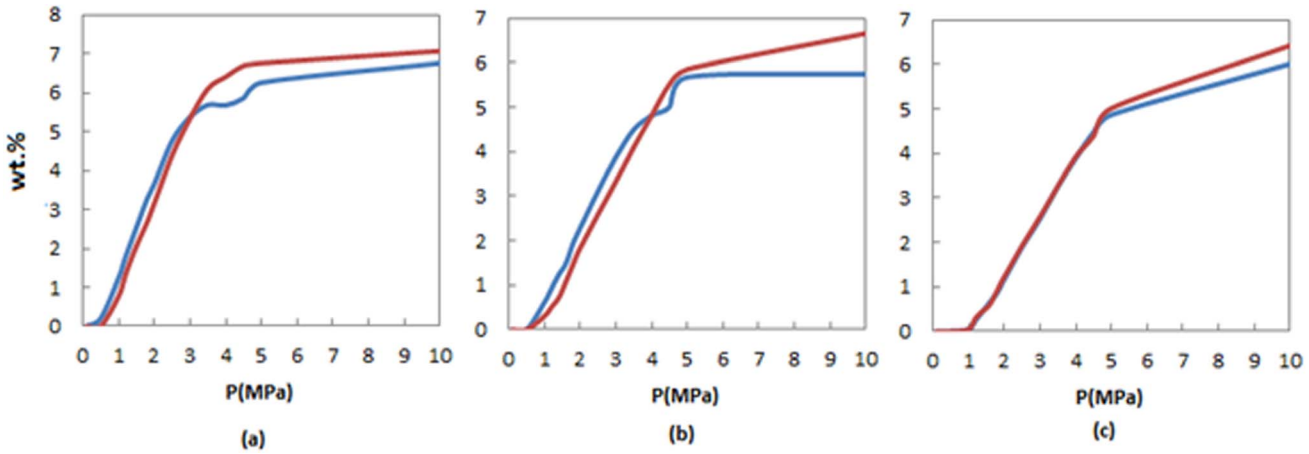

Fig. 4 Comparison of H_2 adsorption isotherms of FeCNT (red line) and pure CNT (blue line) at (a) 175, (b) 250 and (c) 298 K.

Of course, the utilization of molecular dynamics methods in investigating the absorption process in nanostructures should not be disregarded in terms of efficiency and accuracy. For instance, the study of high deposition temperatures, which ensures sufficient surface diffusion of Al and Ga adatoms, has been conducted using AIMD simulation to enhance material quality.[97] The results suggest that the decomposition of graphene layers is attributed to the surface dissociation of $(CH_3)_3Al$ and $(CH_3)_3Ga$, combined with elevated deposition temperatures. Additionally, the behavior of carbon–carbon bonds can be modeled using interatomic potentials such as original Tersoff[98–100] and optimized Tersoff.[101] To predict the mechanical behavior of graphene sheets at the atomic scale, MD simulations have applied an interatomic potential with a modified cutoff function for the Tersoff potential.[102] The use of this modified Tersoff potential has successfully predicted failure stress and strain values that align well with experimentally estimated values.

3.2.2 Radial distribution functions. Radial distribution functions (RDF) of H_2 molecules were calculated around the FeCNT. The density of H_2 molecules, $\rho(r)$, is determined in cylindrical layers at a distance r from the central axis of the CNT. The RDF or $g(r)$ of H_2 around the CNT is defined by the ratio of the local density of H_2 to the bulk density. RDF diagrams in the adsorbent–adsorbate systems show the distribution of gas molecules around the adsorbent. Fig. 5 indicates RDFs of H_2 *versus* r (distance from the central axis of FeCNT) at 298 K and different pressures. The dashed line in 7.07 Å (radius of FeCNT) separates inside and outside RDFs plots. Fig. 4 also shows the snapshot of positions of the center of mass of H_2 molecules outside and inside the FeCNT at 298 K and pressures 1, 2, 5 and 10 MPa, which were generated through equilibrium configurations. The peaks in the density profiles are related to the adsorption phase at a distance of the order of σ_{C-H_2} and σ_{Fe-H_2}, which corresponds to the hydrogen–CNT attractive interaction range. The hydrogen density of the adsorbed phase is greater than the bulk density and outside this distance, it immediately becomes equal to the bulk density.

At lower pressures, 1 MPa (Fig. 5a), the RDFs plots contained only one peak inside the nanotube at about 3 Å from the central axis of CNT. Consequently, at lower pressures, H_2 is adsorbed in a cylindrical layer inside the CNT, which is visible in the simulation snapshot at $P = 1$ MPa. As the pressure increased, an additional peak appeared outside the CNT, which was related to the formation of an adsorbed layer outside the nanotube. The specific trend in the RDF diagrams was comparable to the equilibrium snapshot generated from the FeCNT simulation.

As seen in Fig. 5b, the outside adsorbed H_2 molecules prefer to adsorb on the doped Fe atoms (defect sites) due to the larger interaction energies between the Fe atoms and H_2. This evidence is justified by comparing the Lennard-Jones cross-interaction parameters of Fe–H_2, and C–H_2 (Table 1). Since ε_{Fe-H_2} (0.821 kcal mol^{-1}) is larger than ε_{C-H_2} (0.0764 kcal mol^{-1}), therefore, doped Fe atoms are stronger adsorption sites for H_2 uptake. It has been proven that defect sites in CNTs can absorb hydrogen molecules, which is associated with a significant increase in the interaction energy and affects the storage capacity of CNTs.[103,104]

By comparing RDFs at pressures of 2, 5, and 10 MPa, it is clear that the outer peak increased with increasing pressure. This result was due to the greater adsorption of hydrogen molecules at higher pressures. However, the peak height of inside adsorption remained almost constant with increasing pressure. These results are consistent with the H_2 adsorption isotherms of FeCNT in Fig. 2. It can be observed that the adsorption capacity within the nanotube becomes almost constant at pressures larger than 2 MPa, while the adsorption capacity outside the nanotube exhibits an increasing trend, superior to the inside capacities. This result is due to the repulsion of H_2 molecules at higher pressures and entropy decrease inside the CNT, which are unfavorable conditions for hydrogen adsorption. The outside peak was situated at about 9.5 Å (about 2.45 Å from the CNT wall). There was a minimum potential interaction energy between H_2 molecules and FeCNT at this distance. The location of the outside adsorption layer of H_2 could be determined by the Lennard-Jones parameters, $\sigma_{Fe-H_2} = 2.640$ Å (see Table 1).

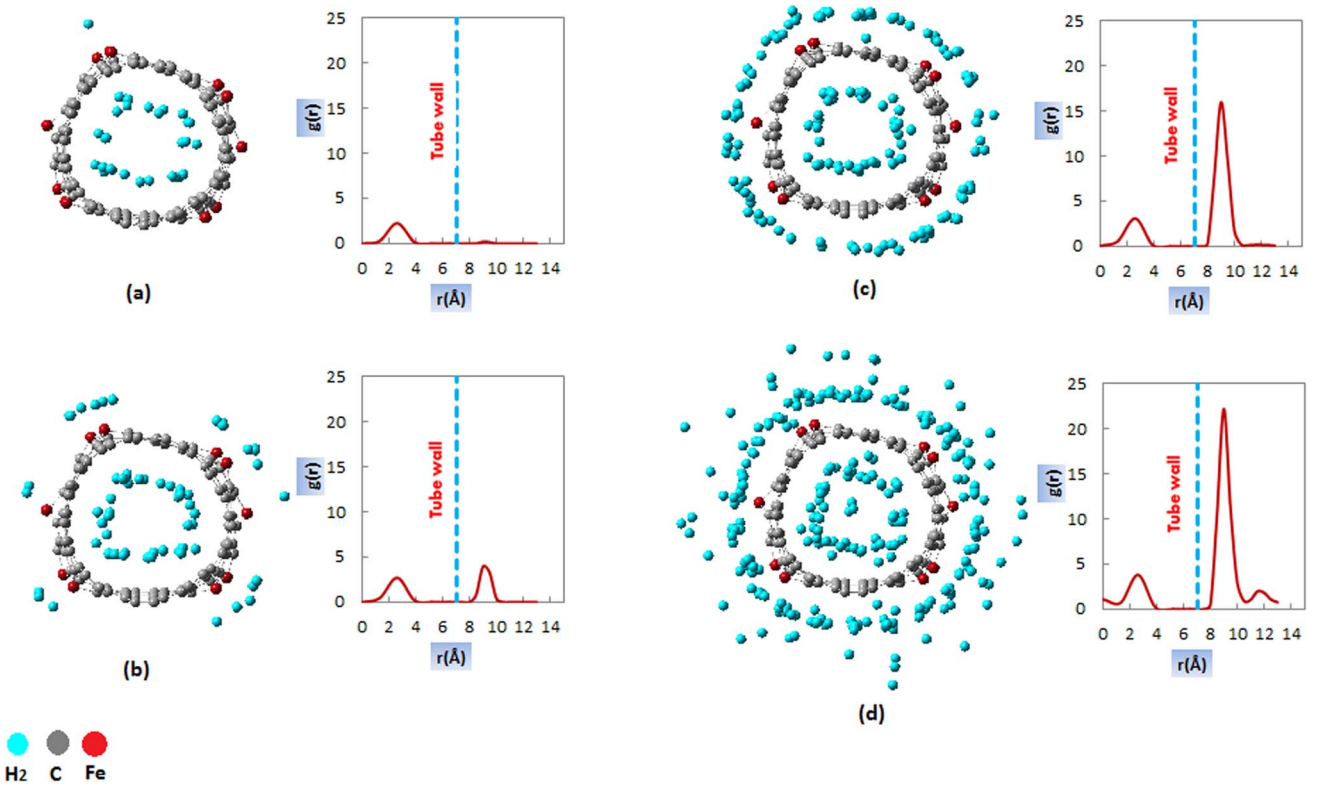

Fig. 5 Radial distribution functions of H_2 molecules inside and outside the FeCNT *versus* distance from the central axis of the nanotube and Snapshot generated by the simulation of hydrogen storage at 298 K and (a) 1 MPa (b) 2 MPa (c) 5 MPa (d) 10 MPa.

By comparing the RDF profiles, it was found that at 10 MPa, another adsorption layer was formed outside the CNT. As can be seen in Fig. 5d, the second adsorption layer occurred in about 12 Å (2.5 Å from the first layer and about 5 Å from the CNT wall). The result was consistent with the isotherm plots which fitted to the Freundlich isotherm model and confirmed the presence of H_2 multi-layer adsorption (see Section 3-2-3). The formation of the second adsorption layer can be recognized in the snapshot generated by the simulation of hydrogen storage at 10 MPa (Fig. 5d).

3.2.3 Analysis of adsorption isotherms. Several adsorption isotherms have been developed to explain and model adsorption processes.[105] The simplest and most convenient isotherm is the Langmuir isotherm.[106] This model assumes that the adsorption is monolayer, the adsorbent surface is homogeneous, the adsorption energy is constant for all adsorption sites, and the adsorbate does not translocate on the surface. In this model every adsorbate molecule can only interact with one adsorption site.

The equation of Langmuir isotherm is as follows:[106,107]

$$q_e = \frac{q_m K_L P}{1 + K_L P} \quad (13)$$

where K_L, P, q_e, and q_m denote the Langmuir adsorption constant, the pressure of adsorbed gas, adsorption uptake at pressure P, and the maximum monolayer adsorption, respectively. The fit of the adsorption isotherms with the Langmuir model can be evaluated by the correlation coefficient of the diagram $1/q_e$ *versus* $1/P$.

Freundlich isotherm can be employed for multilayer adsorption on heterogeneous adsorbent surfaces. This model assumes that the adsorbent surface is heterogeneous, and active sites and their energies are exponentially distributed.[108] In Freundlich isotherm, stronger binding sites are first occupied, until the adsorption energy decreases exponentially after the completion of the adsorption process.[109] The presentation of Freundlich isotherm is considered as following equation:[110]

$$q_e = K_F P^{\frac{1}{n}} \quad (14)$$

where K_F, P and q_e denote the Freundlich adsorption constant, the pressure of adsorbed gas, and adsorption uptake at pressure P, respectively.

H_2 adsorption data on FeCNT were successfully subjected to curve fitting using Langmuir and Freundlich adsorption isotherm model (Fig. 6). The values of Freundlich and Langmuir adsorption isotherm model parameters fitting to the obtained adsorption data are presented in Table 3. The quality of fitting the isotherm models with the obtained adsorption capacities is estimated by the correlation coefficient R^2. As can be seen, using the linear regression method, there is a good matching between the simulation data and the predicted values of the isotherm model with R^2 close to 1. It can be observed that the isotherm at 175 K shows a better fit with the Freundlich model (Fig. 6b, blue line) with $R^2 = 0.9999$ compared to the isotherm at 298 K with R^2

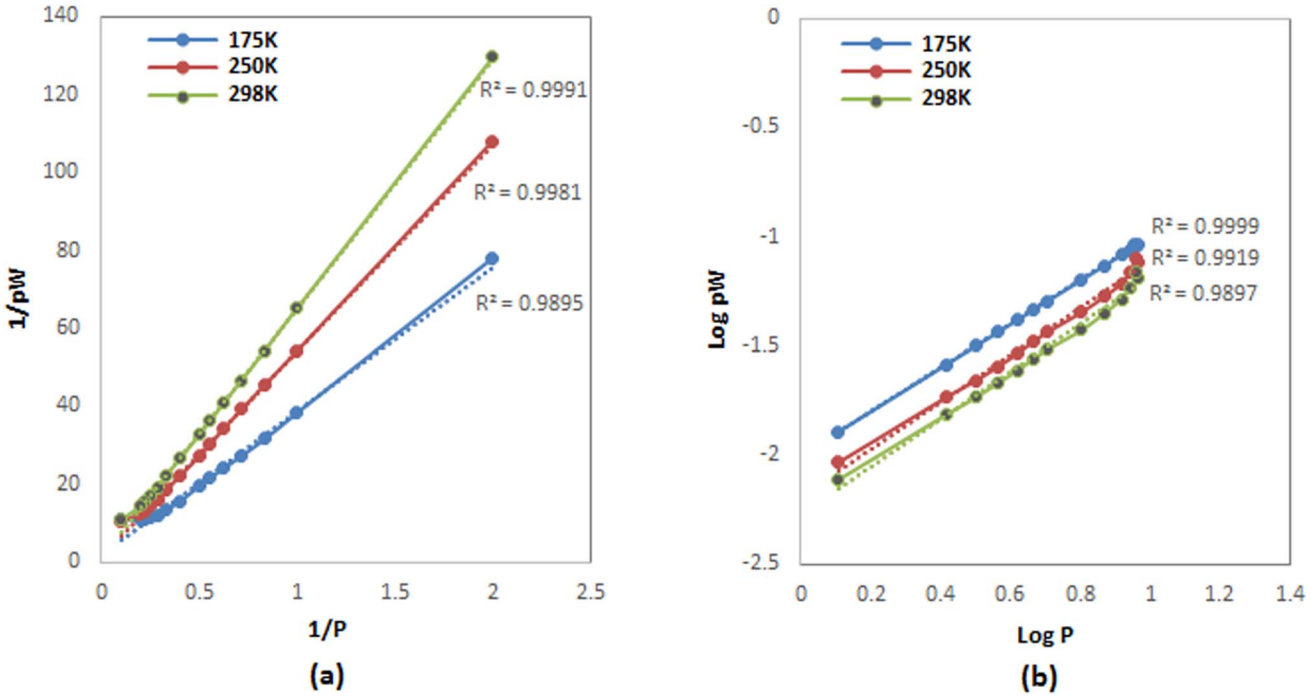

Fig. 6 Fitting isotherms plots for H_2 adsorption at different temperatures (a) Langmuir (b) Freundlich.

Table 3 Langmuir and Freundlich isotherm fitting parameters for H_2 adsorption over FeCNT

	Langmuir parameters		Freundlich parameters	
T (K)	q_m	K_L	K_F	$1/n$
175	0.4452	0.0610	0.0100	1.0031
250	0.5831	0.0325	0.0065	1.0743
298	0.6339	0.0248	0.0054	1.0845

$= 0.9897$, which is an indication of the heterogeneous nature of the adsorption surface (FeCNT). However, the isotherm at 298 K follows the Langmuir model with $R^2 = 0.9991$ better than at 175 K. This evidence is due to Langmuir mono-layer adsorption at higher temperatures. The results are consistent with the isotherm analysis data of the hydrogen storage of CNTs at 303 K and 10 bar[87] which have concluded CNT adsorption data were best fitted by Langmuir isotherm model for monolayer physical adsorption. The maximum adsorption capacity (q_m) values obtained from the Langmuir equation for CNT and B doped CNT were 0.033 and 0.414 wt%, and based on our results, q_m was 0.6339% at 298 K. As can be seen in Table 3, the Langmuir constant (K_L) of FeCNT at 298 K was 0.0248, which is larger than that of CNT (0.0070),[87] confirming that Fe doping plays a major role in hydrogen uptake.

Multilayer H_2 adsorption can occur at lower temperatures due to the high hydrogen storage that causes the formation of a second adsorption layer. Therefore, it is anticipated that the isotherm follows the Freundlich model, and the existence of multi-layer adsorption is proved. This evidence was confirmed by the RDF diagram at 10 MPa, which showed the second adsorption layer outside the nanotube (see Fig. 5d).

3.2.4 Temperature dependence of hydrogen storage. To evaluate the temperature dependence of FeCNT adsorption capacity and to study the H_2 desorption from this adsorbent compared to pure CNT, hydrogen adsorptions of FeCNT and CNT were compared at temperatures 175–350 K under 5 MPa. An increase in temperature can raise the kinetic energy of H_2 molecules, and thus, their interactions with the adsorption sites become weaker. As a result, the rate of desorption increases at higher temperatures. However, the desorption resulting from temperature increment cannot be fully explained by reversibility. Adsorption can occur through different mechanisms, including chemisorption or physisorption, and some structural changes or charge transfers are not reversible with changes in temperature and kinetic energy of adsorbed gas molecules.

Fig. 7 shows the reduction of total adsorption capacity percentage at 5 MPa with raising temperature. As it is seen, pure CNT and FeCNT exhibited the same behavior with increasing temperature. By increasing the temperature from 175 to 298 K, the hydrogen capacity of pure CNT was reduced from 6.75% to 4.84% (storage decrease about 28% of initial capacity). While the hydrogen capacity of FeCNT was reduced from 6.66% to 5.02% (storage decrease about 24% of initial capacity). These results indicated that hydrogen uptake of FeCNT up to 298 K was better than CNT, and therefore hydrogen storage by FeCNT was maintained up to room temperature higher than pure CNT. It is well inferred from Fig. 7 that at temperatures higher than 298 K, the slope of the plot of CNT was lower than that of FeCNT, which indicates its lesser desorption. As the temperature increased from 298 to 350 K, pure CNT and FeCNT

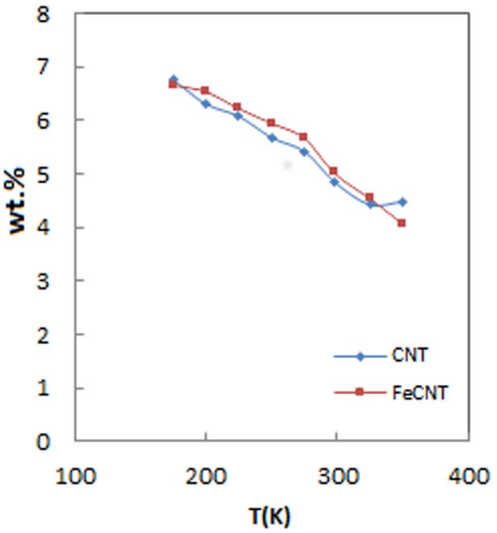

Fig. 7 Variation of H_2 adsorption capacity of FeCNT and pure CNT upon the temperature increment at 5 MPa.

desorbed 7% and 19% of their hydrogen content, respectively. Therefore, it is concluded that with increasing temperature (at temperatures above room temperature), FeCNT shows better reversibility than pure CNT.

3.2.5 H_2/N_2 mixture adsorption. In general, adding N_2 dilutes the H_2 environment and increases the safety of the system, which is more favorable for applications in fuel cells. To investigate the effect of adding N_2 on the H_2 uptake of FeCNT, two gas mixtures with mole fractions of 0.4/0.6 and 0.6/0.4 of H_2/N_2 were chosen.

Fig. 8 shows the dependency of adsorption of H_2/N_2 mixtures on pressure at 298 K. As can be seen, adsorption isotherms for gas mixtures have similar behavior as pure ones. This figure also shows the effect of mole percentage on FeCNT adsorption capacity. As the mole percentage of H_2 in the environment increases, the adsorption capacity increases.

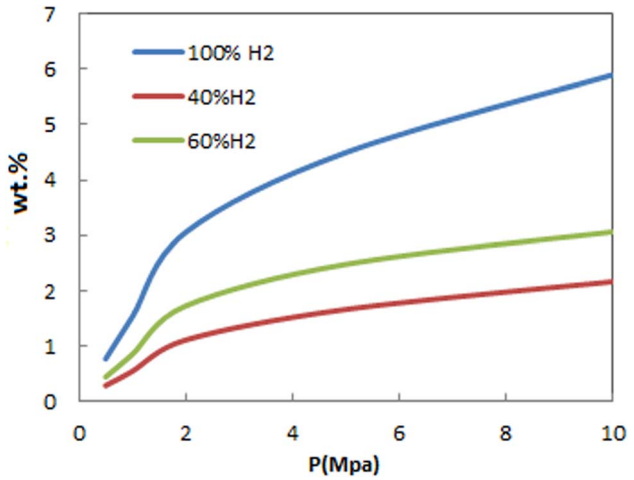

Fig. 8 Comparison of hydrogen adsorption isotherms of FeCNT at 298 K from pure H_2 and H_2/N_2 mixture.

To evaluate the influence of adding N_2 on FeCNT hydrogen storage, adsorption isotherms for H_2 in a gas mixture with N_2 and in the absence of N_2 were investigated. The H_2 adsorption capacities of FeCNT in the gas mixture with N_2 and in the absence of N_2 at 298 K and at selected pressures is tabulated in Table 4. The adsorption capacity of H_2 below 4 MPa in pure and mixture environments was less than 10%, and therefore adding N_2 did not affect the H_2 uptake of FeCNT. Two factors affecting the adsorption capacity are effective pressure and free adsorbent surface. Since the Lennard-Jones parameter ε of N_2 is approximately the same as that of H_2, at lower pressures, adding N_2 to the environment did not change the interactions between H_2 molecules, and therefore did not affect H_2 adsorption. As previously mentioned, N_2 was a diluting agent, and at pressures below 4 MPa, the addition of N_2 to the medium did not significantly affect the hydrogen storage of FeCNT.

At higher pressures, the restriction of the absorption sites because of the absorption of other gases (*i.e.*, N_2) reduces H_2 uptake from the gas mixture. In fact, at higher pressures, absorption depends on the free surface area of the adsorbent, and as a result, adding N_2 to the environment leads to a decrease in the absorption capacity. As a result, pressures below 4 MPa are appropriate for FeCNT hydrogen storage at 298 K from mixed H_2/N_2 systems than higher pressures.

3.2.6 H_2/N_2 selectivity. Due to the significant interest in H_2 adsorption selectivity from gas mixtures, H_2 selectivity from H_2/N_2 mixture was investigated.

The selectivities from the isotherms were calculated by the Ideal Adsorption Solution Theory (IAST),[111] which calculate the gas selectivity of adsorbents from a gas mixture through modeling methods. The selectivity $S_{A/B}$ from a binary gas mixture, A and B, is find out by the following equation:[112,113]

$$S_{A/B} = \frac{X_A / Y_A}{X_B / Y_B} \quad (15)$$

where X and Y are the mole fraction of gas components (A, B) in the adsorbed and bulk phases, respectively. Selectivity is a key parameter to estimate the competitive adsorption between two components. When $S_{A/B} > 1$, component A is favorably adsorbed; whereas $S_{A/B} < 1$, denotes component B is preferentially adsorbed.

Selectivity depends on the strength of adsorbate–adsorbent interactions, pressure, temperature, and gas phase composition. To achieve optimal conditions for H_2 storage from H_2/N_2 mixture, the effects of pressure and composition on the selectivity of FeCNT were investigated.

To determine the H_2/N_2 selectivity of FeCNT, the compositions of 0.1–0.9 mole fraction of H_2/N_2 mixtures at 298 K and pressures up to 10 MPa were considered. The results revealed that H_2 selectivity enhanced with the increase of total bulk pressure for all compositions of H_2 and N_2 mixtures. For instance, the dependence of H_2 selectivity of FeCNT *versus* bulk pressure at 298 K from a H_2/N_2 gas mixture with 60 mol% of H_2 is shown in Fig. 9. As can be seen at lower pressures, S_{H_2/N_2} is lower than 1, and therefore H_2 is not favorably adsorbed.

As seen in Fig. 9, at pressures 2–3 MPa, S_{H_2/N_2} was around 1, which meant that there was no competition. Interactions

Table 4 Comparison of percent adsorption capacities of FeCNT in pure H_2 and H_2/N_2 mixture in different mole percent environments at 298 K

	40% H_2		60% H_2	
P (MPa)	wt% (H_2) in pure H_2	wt% (H_2) in H_2/N_2 mixture	wt% (H_2) in pure H_2	wt% (H_2) in H_2/N_2 mixture
0.5	0.310	0.2909	0.4646	0.4453
1	0.6185	0.5480	0.9247	0.8538
2	1.2277	1.1131	1.8396	1.7280
3	1.8367	1.6652	2.7405	2.4799
4	2.4263	2.1657	3.6339	3.0612
5	3.0477	2.4214	4.4780	3.6780
10	5.6833	4.0827	7.6962	5.2460

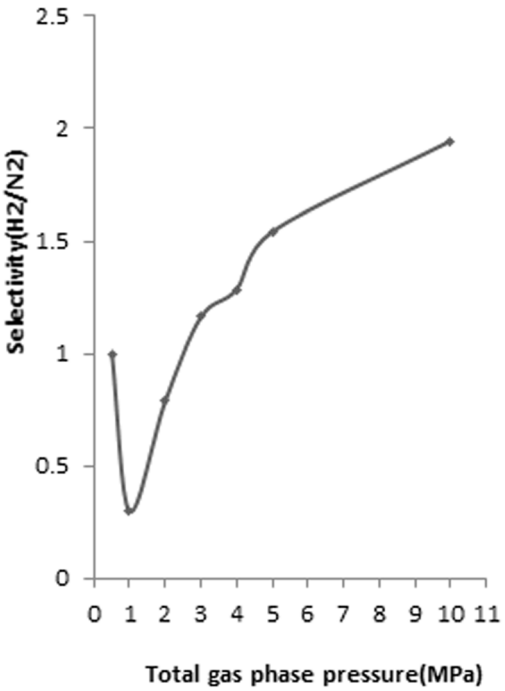

Fig. 9 H_2 selectivity of FeCNT from mixture of 60 mol% H_2/N_2 *vs.* pressure at 298 K (mole fraction of 0.6 H_2 and 0.4 N_2 mixtures).

between gas molecules and NT affect selectivity values.[114] The slightly larger H_2–Fe and Fe–C interactions compared to N_2–Fe and N_2–C (see Table 1), leads to nearly identical selectivity of H_2 and N_2 at lower pressures. At pressures greater than 3 MPa, H_2/N_2 selectivity tends to be larger than 1, and therefore H_2 is efficiently adsorbed. This selectivity is due to the different affinity of the H_2 and N_2 for adsorbing on the CNT.

Furthermore, it is expected that smaller molecules can be better packed into the CNTs at higher pressures. This fact has been also found in carbon membranes.[70] An effective factor in increasing the adsorption capacity with increasing pressure is the packing effect.[115]

Indeed, in the present study, the smaller kinetic diameter of H_2 (0.24 A) compared to N_2 (0.36 A)[116] leads to higher diffusion and higher selectivity of H_2 over N_2 in FeCNT, especially at higher pressures. Accordingly, due to superior hydrogen uptake from H_2/N_2 gas mixtures, pressures larger than 3 MPa are convenient. As can be seen in Fig. 10, at low pressures, the selectivity of H_2 is smaller than that of N_2 and then enhances along with increasing pressure. The effect of pressure on the selectivity of CH_4 over H_2 on SiNTs has displayed the same trend.[117] As mentioned, smaller molecules are more appropriate for packing in the CNT, the selectivity of CH_4/H_2 decreases with increasing pressure.

As it is noticed, in addition to the effect of the relative diameters of the two gases, H_2/N_2 selectivity depends on the structure of the adsorbent and the strength of the interaction of H_2 and N_2 with the adsorption sites. In a recent study, adsorption of pure H_2 or N_2 and H_2/N_2 mixture in SIFSIX-2-Cu-I has been investigated through Monte Carlo simulation using the polarizable force field[118] SIFSIX-2-Cu-I is synthesized by organic ligands, metal nodes, and hexafluorosilicate (SiF_6^{2-}) anions. Since N_2 molecules have a denser electron cloud distribution

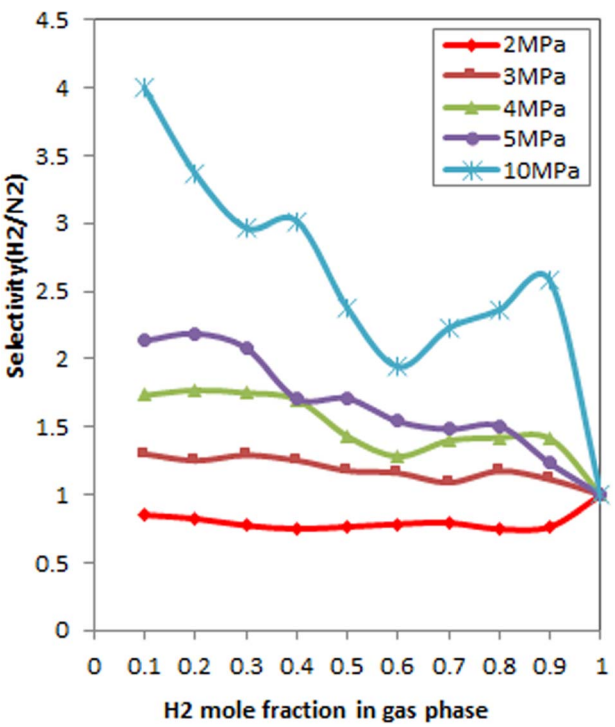

Fig. 10 Selectivity of H_2/N_2 as a function of H_2 bulk composition at 298 K and different pressures.

(than H_2), F atoms have a higher affinity for N_2 molecules. Therefore, selectivity for N_2 over H_2 has been observed in SIFSIX-2-Cu-i.

In another investigation, polysulfone membrane provided H_2/N_2 selectivity of 0.76, and mixing it with low concentrations of carbon nanotubes led to an increase in H_2/N_2 selectivity up to 3.95. These remarkable results are due to the increase in free volume, molecular space, and H_2 absorption.[119] The trend of H_2/N_2 selectivity of CNT/polysulfone membrane *versus* pressure was consistent with our outcomes.

The primary objective of this research was to investigate the efficiency of Fe doping in the hydrogen adsorption properties of CNTs. In this regard, we have also compared FeCNT and CNT by evaluating their H_2 selectivity in an H_2/N_2 mixture environment.

To assess the selectivity performance of CNT and FeCNT, H_2/N_2 selectivity at different bulk compositions was determined at 5 and 298 K, as shown in Table 5. Considering that the adsorption capacity of FeCNT is greater than that of CNT at pressures larger than 4.5 MPa, the selectivity performance of FeCNT relative to CNT was examined at 5 MPa.

As seen in Table 5, the H_2/N_2 selectivity of FeCNT is greater than CNT and greater than 1, indicating efficient H_2 adsorption by FeCNT at 5 and 298 K. On the other hand, the H_2/N_2 selectivity of CNT is smaller than 1 in almost all studied bulk compositions (except $X(H_2) = 0.6$), indicating that CNT cannot preferentially adsorb H_2 over N_2.

Fig. 10 denotes the effect of the bulk mole fraction of H_2 on the selectivity of H_2/N_2 at 298 K and different pressures. As can be seen, selectivity improves with increasing pressure. This result is due to the packing effect, which prevails with increasing pressure. Since the packing effect of H_2 is greater than that of N_2 due to its smaller kinetic diameter,[116] as the pressure changes, the selectivity is enhanced significantly. The combination of increasing H_2 mole fraction in the gas phase and the adsorption sieve effect increases H_2 selectivity.

At 3 MPa, S_{H_2/N_2} was equal to 1 in all mole fractions, and it did not change much with the bulk phase composition change. This is because there was no competition, and thus the bulk composition did not affect the H_2 selectivity at 3 MPa.

Thus, the pressure of 4 and 5 MPa in which the FeCNT shows an adsorption preference for H_2 over the wide range of bulk mole fractions can be considered as an optimum pressure.

As mentioned earlier, at pressures greater than 5 MPa, FeCNT was approximately saturated. Therefore, at 10 MPa, it is reasonable to see a decrease in selectivity with an increasing mole fraction of H_2.

Fig. 10 shows that the maximum selectivity of H_2/N_2 was stated at 0.3 bulk mole fraction of H_2 at 5 MPa. However, as previously mentioned, the selectivity increases with increasing pressure and at 10 MPa, FeCNT has the highest values for H_2/N_2 selectivity. Therefore based on the obtained results, the proposed optimum conditions for H_2 selectivity in H_2/N_2 mixtures were $X(H_2) = 0.3$ at 5 MPa, $X(H_2) = 0.4$ at 4 MPa, and all mole fractions at 10 MPa.

Consequently, considering the result of Section 3.2, which mentioned that adding N_2 to the environment does not have a significant effect on FeCNT hydrogen adsorption at pressures below 4 MPa, the composition of $X(H_2) = 0.4$ and pressure of 4 MPa is suggested as the most effective adsorption condition.

Table 5 Comparison of H_2/N_2 selectivity of CNT and FeCNT in different bulk compositions at 5 MPa and 298 K

H_2 mole fraction in gas phase	Selectivity (H_2/N_2)	
	FeCNT	CNT
0.2	2.19	0.32
0.3	2.08	0.50
0.4	1.71	0.73
0.5	1.71	0.91

4. Conclusion

Considering the ability of metals to absorb hydrogen, it was valuable to study the absorption capacity of new nanomaterials created by metal doping on the surface of other nanomaterials. Consequently, this research focused on evaluating the potential of FeCNT for H_2 storage. Monte Carlo simulation was performed to compare the adsorption behavior of FeCNT and investigate the effects of temperature, pressure, and bulk mole fraction of H_2 on FeCNT adsorption capacity. Temperature range of 75–350 K and pressure range of 0.5–10 MPa were considered. The simulation results showed that all adsorption isotherms exhibited a similar trend, and at pressures of about 5 MPa and above, FeCNT showed maximum hydrogen capacity.

At a constant bulk pressure, increasing the mole fraction of H_2 in the gas phase increased the adsorption capacity. The Comparison of hydrogen capacities at increasing temperatures showed that the reversibility of FeCNT was more efficient than pure CNT above ambient conditions.

The results of adding N_2 to the medium as a diluent for system safety revealed that hydrogen uptake of FeCNT did not change considerably under 4 MPa, and it has the potential to efficiently adsorb H_2 molecules at 298 K from H_2/N_2 mixture. Since both H_2 and N_2 are non-polar small molecules, the selectivity of H_2 from the H_2/N_2 mixture was of great interest in this research.

The outcomes of the current research revealed that the H_2 storage of CNT is enhanced by Fe doping at pressures above 4.5 MPa, and Fe-doping of CNT can be considered a viable strategy for achieving efficient H_2 storage at larger pressures. Moreover, the comparison of H_2/N_2 selectivity performance of FeCNT and CNT at different bulk compositions and pressures larger than 4.5 MPa indicated that the selectivity of FeCNT is greater than CNT and greater than 1 which confirms FeCNT can preferentially adsorb H_2 over N_2. As a result, FeCNT is more suitable than pure CNT for hydrogen storage applications because of its improved hydrogen adsorption capacity and can also be used as a potential candidate for efficient H_2/N_2 adsorption.

Author contributions

Sepideh Ketabi: supervised, data analysis, visualization, writing (original draft & editing), Bita Baghai: performing simulation, methodology, data collection, the whole manuscript was approved by all authors.

Conflicts of interest

The authors declare that they have no known competing financial interests or personal relationships that could have appeared to influence the work reported in this paper.

References

1 M. Höök and X. Tang, Depletion of fossil fuels and anthropogenic climate change—A review, *Energy Policy*, 2013, **52**, 797–809.
2 L. Schlapbach and A. Züttel, Hydrogen-storage materials for mobile applications, *nature*, 2001, **414**(6861), 353–358.
3 G. Mpourmpakis, E. Tylianakis and G. E. Froudakis, Carbon nanoscrolls: a promising material for hydrogen storage, *Nano Lett.*, 2007, **7**(7), 1893–1897.
4 A. Bilic and J. D. Gale, Chemisorption of molecular hydrogen on carbon nanotubes: a route to effective hydrogen storage?, *J. Phys. Chem. C*, 2008, **112**(32), 12568–12575.
5 B. Fang, H. Zhou and I. Honma, Ordered porous carbon with tailored pore size for electrochemical hydrogen storage application, *J. Phys. Chem. B*, 2006, **110**(10), 4875–4880.
6 J. Vajo, F. Pinkerton and N. Stetson, Nanoscale phenomena in hydrogen storage, *Nanotechnology*, 2009, **20**(20), 200201.
7 M. Zafar, T. Iqbal, S. Fatima, Q. Sanaullah and S. Aman, Carbon nanotubes for production and storage of hydrogen: challenges and development, *Chem. Pap.*, 2021, 1–17.
8 Y. Cheng, X. Ma, C. Huang, G. Yuan and J. Liao, The effect of functional groups (O, F, or OH) on reversible hydrogen storage properties of Ti2X (X= C or N) monolayer, *Int. J. Hydrogen Energy*, 2022, **47**(67), 28969–28977.
9 K. Shivaprasad, S. Raviteja, P. Chitragar and G. Kumar, Experimental investigation of the effect of hydrogen addition on combustion performance and emissions characteristics of a spark ignition high speed gasoline engine, *Proc. Technol.*, 2014, **14**, 141–148.
10 P. M. Ajayan, Nanotubes from carbon, *Chem. Rev.*, 1999, **99**, 1787–1799.
11 S. Iijima, Growth of carbon nanotubes, *Mater. Sci. Eng. B*, 1993, **19**(1–2), 172–180.
12 G. Korneva, *Functionalization of Carbon Nanotubes*, Drexel University, 2008.
13 A. Amiri, M. Maghrebi, M. Baniadam and S. Z. Heris, One-pot, efficient functionalization of multi-walled carbon nanotubes with diamines by microwave method, *Appl. Surf. Sci.*, 2011, **257**(23), 10261–10266.
14 Y. Itas, C. Ndikilar and T. Zangina, Carbon nanotubes: a review of synthesis and characterization methods/techniques, *Int. J. Sci. Technoledge*, 2020, **8**(2), 43–51.
15 Y. S. Itas, C. E. Ndikilar, T. Zangina, H. Y. Hafeez, A. Safana, M. U. Khandaker, P. Ahmad, I. Abdullahi, B. K. Olawumi and M. A. Babaji, Synthesis of thermally stable h-BN-CNT hetero-structures *via* microwave heating of ethylene under nickel, iron, and silver catalysts, *Crystals*, 2021, **11**(9), 1097.
16 A. Dalton, C. Stephan, J. Coleman, B. McCarthy, P. Ajayan, S. Lefrant, P. Bernier, W. Blau and H. Byrne, Selective interaction of a semiconjugated organic polymer with single-wall nanotubes, *J. Phys. Chem. B*, 2000, **104**(43), 10012–10016.
17 T. Ramanathan, F. Fisher, R. Ruoff and L. C. Brinson, Amino-functionalized carbon nanotubes for binding to polymers and biological systems, *Chem. Mater.*, 2005, **17**(6), 1290–1295.
18 F. Rumiche, H. Wang and J. Indacochea, Development of a fast-response/high-sensitivity double wall carbon nanotube nanostructured hydrogen sensor, *Sens. Actuators, B*, 2012, **163**(1), 97–106.
19 J.-M. Tulliani, A. Cavalieri, S. Musso, E. Sardella and F. Geobaldo, Room temperature ammonia sensors based on zinc oxide and functionalized graphite and multi-walled carbon nanotubes, *Sens. Actuators, B*, 2011, **152**(2), 144–154.
20 L. Sun, X. Wang, Y. Wang and Q. Zhang, Roles of carbon nanotubes in novel energy storage devices, *Carbon*, 2017, **122**, 462–474.
21 S. A. Yamusa, A. Shaari, I. Isah, U. B. Ibrahim, S. I. Kunya, S. Abdulkarim, Y. Itas and M. Alsalamh, Effects of exchange correlation functional (Vwdf3) on the structural, elastic, and electronic properties of transition metal dichalogenides, *J. Niger. Soc. Phys. Sci.*, 2023, 1094.
22 J. H. Cho, S. J. Yang, K. Lee and C. R. Park, Si-doping effect on the enhanced hydrogen storage of single walled carbon nanotubes and graphene, *Int. J. Hydrogen Energy*, 2011, **36**(19), 12286–12295.
23 A. Salimian, S. Ketabi and H. Aghabozorg, Hydrogen adsorption capacity of vanadium oxide nanotube from pure and mixture gas environment through molecular simulation, *Sep. Sci. Technol.*, 2018, **53**(1), 1–12.
24 J. Wu, Doping Modification of Carbon Nanotubes and its Applications, *Highlights in Science, Engineering and Technology*, 2022, **27**, 327–333.
25 A. Gholizadeh and B. Dehbandi, First-principles study on structural, electronic, and magnetic properties of 3d transition metal-substituted chiral (6, 3) carbon nanotube, *Comput. Condens. Matter*, 2022, **30**, e00621.
26 S. Banerjee, K. Dasgupta, A. Kumar, P. Ruz, B. Vishwanadh, J. Joshi and V. Sudarsan, Comparative evaluation of hydrogen storage behavior of Pd doped carbon nanotubes prepared by wet impregnation and polyol methods, *Int. J. Hydrogen Energy*, 2015, **40**(8), 3268–3276.
27 C.-H. Chen, T.-Y. Chung, C.-C. Shen, M.-S. Yu, C.-S. Tsao, G.-N. Shi, C.-C. Huang, M.-D. Ger and W.-L. Lee, Hydrogen storage performance in palladium-doped

graphene/carbon composites, *Int. J. Hydrogen Energy*, 2013, **38**(9), 3681–3688.
28 I. Mosquera-Lois, S. R. Kavanagh, J. Klarbring, K. Tolborg and A. Walsh, Imperfections are not 0 K: free energy of point defects in crystals, *Chem. Soc. Rev.*, 2023, **52**, 5812–5826.
29 A. Salimian, S. Ketabi and H. Aghabozorg, Hydrogen storage comparison of M doped vanadium oxide nanotubes (M= Mo, Zr and W): A molecular simulation study, *Int. J. Hydrogen Energy*, 2018, **43**(5), 2831–2839.
30 B. I. Kharisov, O. V. Kharissova, U. Ortiz Mendez and I. G. De La Fuente, Decoration of carbon nanotubes with metal nanoparticles: Recent trends, *Synthesis and Reactivity in Inorganic, Metal-Organic, and Nano-Metal Chemistry*, 2016, **46**(1), 55–76.
31 F. A. Jibon, M. U. Khandaker, M. H. Miraz, H. Thakur, F. Rabby, N. Tamam, A. Sulieman, Y. S. Itas and H. Osman, Cancerous and non-cancerous brain MRI classification method based on convolutional neural network and log-polar transformation, *Healthcare*, 2022, 1801.
32 Y. Yürüm, A. Taralp and T. N. Veziroglu, Storage of hydrogen in nanostructured carbon materials, *Int. J. Hydrogen Energy*, 2009, **34**(9), 3784–3798.
33 A. Dadgar, A. Maleki, L. Mahdavian and F. Khazali, Computational and structural study of titanium/carbon nanotube nanocomposite, *Diamond Relat. Mater.*, 2022, **126**, 109055.
34 R. Rakhi, K. Sethupathi and S. Ramaprabhu, Synthesis and hydrogen storage properties of carbon nanotubes, *Int. J. Hydrogen Energy*, 2008, **33**(1), 381–386.
35 M. Kumar and Y. Ando, Chemical vapor deposition of carbon nanotubes: a review on growth mechanism and mass production, *J. Nanosci. Nanotechnol.*, 2010, **10**(6), 3739–3758.
36 K.-S. Lin, Y.-J. Mai, S.-R. Li, C.-W. Shu and C.-H. Wang, Characterization and hydrogen storage of surface-modified multiwalled carbon nanotubes for fuel cell application, *J. Nanomater.*, 2012, **2012**, 13.
37 H.-M. Cheng, Q.-H. Yang and C. Liu, Hydrogen storage in carbon nanotubes, *Carbon*, 2001, **39**(10), 1447–1454.
38 A. Reyhani, S. Mortazavi, S. Mirershadi, A. Moshfegh, P. Parvin and A. N. Golikand, Hydrogen storage in decorated multiwalled carbon nanotubes by Ca, Co, Fe, Ni, and Pd nanoparticles under ambient conditions, *J. Phys. Chem. C*, 2011, **115**(14), 6994–7001.
39 Y. Suttisawat, P. Rangsunvigit, B. Kitiyanan, M. Williams, P. Ndungu, M. Lototskyy, A. Nechaev, V. Linkov and S. Kulprathipanja, Investigation of hydrogen storage capacity of multi-walled carbon nanotubes deposited with Pd or V, *Int. J. Hydrogen Energy*, 2009, **34**(16), 6669–6675.
40 S.-U. Rather, N. Mehraj-ud-din, R. Zacharia, S. W. Hwang, A. R. Kim and K. S. Nahm, *Int. J. Hydrogen Energy*, 2009, **34**, 961–966.
41 V. Kiselev and O. Krylov, Adsorption and Catalysis of Transition Metals and their Oxides, *Indian J. Phys.*, 1993, **67**, 201–206.
42 A. Lueking and R. T. Yang, Hydrogen spillover from a metal oxide catalyst onto carbon nanotubes—implications for hydrogen storage, *J. Catal.*, 2002, **206**(1), 165–168.
43 L. Gao, E. Yoo, J. Nakamura, W. Zhang and H. T. Chua, Hydrogen storage in Pd–Ni doped defective carbon nanotubes through the formation of CHx (x= 1, 2), *Carbon*, 2010, **48**(11), 3250–3255.
44 A. Sharma, Investigation on platinum loaded multi-walled carbon nanotubes for hydrogen storage applications, *Int. J. Hydrogen Energy*, 2020, **45**(4), 2967–2974.
45 M. Aghababaei, A. A. Ghoreyshi and K. Esfandiari, Optimizing the conditions of multi-walled carbon nanotubes surface activation and loading metal nanoparticles for enhanced hydrogen storage, *Int. J. Hydrogen Energy*, 2020, **45**(43), 23112–23121.
46 A. Dhanya, N. Ranjan and S. Ramaprabhu, Hydrogen storage studies of Co, Fe, Fe3C nanoparticles encapsulated nitrogen doped carbon nanotubes, *Energy Storage*, 2023, **5**(4), e421.
47 E. Dündar-Tekkaya and N. Karatepe, Hydrogen adsorption of carbon nanotubes grown on different catalysts, *Int. J. Hydrogen Energy*, 2015, **40**(24), 7665–7670.
48 M. Yoosefian and N. Etminan, Pd-doped single-walled carbon nanotube as a nanobiosensor for histidine amino acid, a DFT study, *RSC Adv.*, 2015, **5**(39), 31172–31178.
49 K. Li, W. Wang and D. Cao, Novel chemical sensor for CO and NO: silicon nanotube, *J. Phys. Chem. C*, 2011, **115**(24), 12015–12022.
50 S. C. Lim, J. H. Jang, D. J. Bae, G. H. Han, S. Lee, I.-S. Yeo and Y. H. Lee, Contact resistance between metal and carbon nanotube interconnects: Effect of work function and wettability, *Appl. Phys. Lett.*, 2009, **95**(26), 264103.
51 L. An, X. Jia and Y. Liu, Adsorption of SO_2 molecules on Fe-doped carbon nanotubes: The first principles study, *Adsorption*, 2019, **25**, 217–224.
52 N. Luhadiya, V. Choyal, S. I. Kundalwal and S. Sahu, Investigation of unified impact of Ti adatom and N doping on hydrogen gas adsorption capabilities of defected graphene sheets, *J. Mol. Graph. Model.*, 2023, **119**, 108399.
53 D. G. Sangiovanni, R. Faccio, G. K. Gueorguiev and A. Kakanakova-Georgieva, Discovering atomistic pathways for supply of metal atoms from methyl-based precursors to graphene surface, *Phys. Chem. Chem. Phys.*, 2023, **25**(1), 829–837.
54 A. P. Pandey, M. Shaz, V. Sekkar and R. Tiwari, Synergistic effect of CNT bridge formation and spillover mechanism on enhanced hydrogen storage by iron doped carbon aerogel, *Int. J. Hydrogen Energy*, 2023, **48**(56), 21395–21403.
55 Y. Pan, Y. Liu, Y. Lin and C. Liu, Metal doping effect of the M–Co2P/Nitrogen-Doped carbon nanotubes (M= Fe, Ni, Cu) hydrogen evolution hybrid catalysts, *ACS Appl. Mater. Interfaces*, 2016, **8**(22), 13890–13901.
56 Y. S. Itas, M. U. Khandaker, A. B. Suleiman, C. E. Ndikilar, A. Lawal, R. Razali, I. I. Idowu, A. M. Danmadami, A. S. Yamusa and H. Osman, Studies of H_2 storage efficiency of metal-doped carbon nanotubes by optical

adsorption spectra analysis, *Diamond Relat. Mater.*, 2023, **136**, 109964.
57 F. Tang, W. Xia, H. Zhang, L. Zheng, Y. Zhao, J. Ge and J. Tang, Synthesis of Fe-doped carbon hybrid composed of CNT/flake-like carbon for catalyzing oxygen reduction, *Nano Res.*, 2022, **15**(7), 6670–6677.
58 Z. Wang, G. Wei and G. L. Zhao, Enhanced electromagnetic wave shielding effectiveness of Fe doped carbon nanotubes/epoxy composites, *Appl. Phys. Lett.*, 2013, **103**(18), 183109.
59 Y. Liu, H. Zhang, Z. Zhang, X. Jia and L. An, CO adsorption on Fe-doped vacancy-defected CNTs–A DFT study, *Chem. Phys. Lett.*, 2019, **730**, 316–320.
60 Y. Liu, V. I. Artyukhov, M. Liu, A. R. Harutyunyan and B. I. Yakobson, Feasibility of lithium storage on graphene and its derivatives, *J. Phys. Chem. Lett.*, 2013, **4**(10), 1737–1742.
61 K. Persson, Y. Hinuma, Y. S. Meng, A. Van der Ven and G. Ceder, Thermodynamic and kinetic properties of the Li-graphite system from first-principles calculations, *Phys. Rev. B: Condens. Matter Mater. Phys.*, 2010, **82**(12), 125416.
62 L. Zhao, C. Chai, W. Petz and G. Frenking, Carbones and carbon atom as ligands in transition metal complexes, *Molecules*, 2020, **25**(21), 4943.
63 C. Bittencourt, A. Felten, J. Ghijsen, J.-J. Pireaux, W. Drube, R. Erni and G. Van Tendeloo, Decorating carbon nanotubes with nickel nanoparticles, *Chem. Phys. Lett.*, 2007, **436**(4–6), 368–372.
64 J. P. Perdew, K. Burke and M. Ernzerhof, Generalized gradient approximation made simple, *Phys. Rev. Lett.*, 1996, **77**(18), 3865.
65 Q. Wang, Y.-J. Liu and J.-X. Zhao, Theoretical study on the encapsulation of Pd 3-based transition metal clusters inside boron nitride nanotubes, *J. Mol. Model.*, 2013, **19**, 1143–1151.
66 P. Giannozzi, S. Baroni, N. Bonini, M. Calandra, R. Car, C. Cavazzoni, D. Ceresoli, G. L. Chiarotti, M. Cococcioni and I. Dabo, QUANTUM ESPRESSO: a modular and open-source software project for quantum simulations of materials, *J. Condens. Matter Phys.*, 2009, **21**(39), 395502.
67 N. Metropolis, A. W. Rosenbluth, M. N. Rosenbluth, A. H. Teller and E. Teller, Equation of state calculations by fast computing machines, *J. Chem. Phys.*, 1953, **21**(6), 1087–1092.
68 J. Estela-Uribe, J. Jaramillo, M. Salazar and J. Trusler, Virial equation of state for natural gas systems, *Fluid Ph. Equilib.*, 2003, **204**(2), 169–182.
69 M. Jaeschke and A. Humphreys, *The GERG Databank of High Accuracy Compressibility Measurements*, GERG Tech. Monograph, vol. 4, 1990.
70 Y. Jia, M. Wang, L. Wu and C. Gao, Separation of CO2/N2 gas mixture through carbon membranes: Monte Carlo simulation, *Sep. Sci. Technol.*, 2007, **42**(16), 3681–3695.
71 A. K. Rappé, C. J. Casewit, K. Colwell, W. A. Goddard III and W. M. Skiff, UFF, a full periodic table force field for molecular mechanics and molecular dynamics simulations, *J. Am. Chem. Soc.*, 1992, **114**(25), 10024–10035.
72 K. Malek and M. Sahimi, Molecular dynamics simulations of adsorption and diffusion of gases in silicon-carbide nanotubes, *J. Chem. Phys.*, 2010, **132**(1), 014310.
73 J. I. Paredes, F. Suárez-García, S. Villar-Rodil, A. Martínez-Alonso, J. M. Tascón and E. J. Bottani, N2 physisorption on carbon nanotubes: computer simulation and experimental results, *J. Phys. Chem. B*, 2003, **107**(34), 8905–8916.
74 E. Bottani and V. Bakaev, The grand canonical ensemble Monte Carlo simulation of nitrogen on graphite, *Langmuir*, 1994, **10**(5), 1550–1555.
75 J.-P. Hansen and I. R. McDonald, *Theory of Simple Liquids: with Applications to Soft Matter*, Academic press, 2013.
76 A. R. Leach, *Molecular Modelling: Principles and Applications*, Pearson education, 2001.
77 R. Bian, J. Zhao and H. Fu, Silicon–doping in carbon nanotubes: formation energies, electronic structures, and chemical reactivity, *J. Mol. Model.*, 2013, **19**, 1667–1675.
78 T. T. H. Nguyen, C. Le Minh and N. H. Nguyen, A theoretical study of carbon dioxide adsorption and activation on metal-doped (Fe, Co, Ni) carbon nanotube, *Comput. Theor. Chem.*, 2017, **1100**, 46–51.
79 X.-X. Wang, X.-Y. Li and H.-N. Li, First principles study of Eu doped carbon nanotubes, *Phys. Lett. A*, 2008, **372**(44), 6677–6680.
80 Y. Yagi, T. M. Briere, M. H. Sluiter, V. Kumar, A. A. Farajian and Y. Kawazoe, Stable geometries and magnetic properties of single-walled carbon nanotubes doped with 3 d transition metals: A first-principles study, *Phys. Rev. B: Condens. Matter Mater. Phys.*, 2004, **69**(7), 075414.
81 W. Zhang, F. Zhang, Z. Zhang, S. Lu and Y. Yang, Electronic structure and magnetism of Fe-doped SiC nanotubes, *Sci. China: Phys. Mech. Astron.*, 2010, **53**, 1582–1589.
82 T. Yildirim, J. Íñiguez and S. Ciraci, Molecular and dissociative adsorption of multiple hydrogen molecules on transition metal decorated C 60, *Phys. Rev. B: Condens. Matter Mater. Phys.*, 2005, **72**(15), 153403.
83 J. Toth, *Adsorption*, CRC Press, 2002.
84 A. A. Rafati, S. M. Hashemianzadeh, Z. B. Nojini and N. Naghshineh, Canonical Monte Carlo simulation of adsorption of O2 and N2 mixture on single walled carbon nanotube at different temperatures and pressures, *J. Comput. Chem.*, 2010, **31**(7), 1443–1449.
85 U.D.o. Energy, *DOE Technical Targets for Onboard Hydrogen Storage for Light-Duty Vehicles*, 2017.
86 P. García-Holley, B. Schweitzer, T. Islamoglu, Y. Liu, L. Lin, S. Rodriguez, M. H. Weston, J. T. Hupp, D. A. Gómez-Gualdrón and T. Yildirim, Benchmark study of hydrogen storage in metal–organic frameworks under temperature and pressure swing conditions, *ACS Energy Lett.*, 2018, **3**(3), 748–754.
87 S. V. Sawant, S. Banerjee, A. W. Patwardhan, J. B. Joshi and K. Dasgupta, Effect of in-situ boron doping on hydrogen adsorption properties of carbon nanotubes, *Int. J. Hydrogen Energy*, 2019, **44**(33), 18193–18204.

88 W. Liu, Y. Zhao, Y. Li, Q. Jiang and E. Lavernia, Enhanced hydrogen storage on Li-dispersed carbon nanotubes, *J. Phys. Chem. C*, 2009, **113**(5), 2028–2033.
89 Y.-J. Han and S.-J. Park, Influence of nickel nanoparticles on hydrogen storage behaviors of MWCNTs, *Appl. Surf. Sci.*, 2017, **415**, 85–89.
90 S. Kaskun and M. Kayfeci, The synthesized nickel-doped multi-walled carbon nanotubes for hydrogen storage under moderate pressures, *Int. J. Hydrogen Energy*, 2018, **43**(23), 10773–10778.
91 M. Konni, N. Narayanam, A. S. Dadhich and S. B. Mukkamala, Effect of Reaction Media on Hydrogen Sorption Properties of Mg-Decorated MWCNTs, *Fullerenes, Nanotubes and Carbon Nanostructures*, 2015, **23**(9), 782–787.
92 M. Konni, A. S. Dadhich and S. B. Mukkamala, Impact of surface modifications on hydrogen uptake by Fe@ f-MWCNTs and Cu@ f-MWCNTs at non-cryogenic temperatures, *Int. J. Hydrogen Energy*, 2017, **42**(2), 953–959.
93 S. ullah Rather, Hydrogen uptake of cobalt and copper oxide-multiwalled carbon nanotube composites, *Int. J. Hydrogen Energy*, 2017, **42**(16), 11553–11559.
94 D. Silambarasan, V. Surya, V. Vasu and K. Iyakutti, Investigation of single-walled carbon nanotubes-titanium metal composite as a possible hydrogen storage medium, *Int. J. Hydrogen Energy*, 2013, **38**(34), 14654–14660.
95 P. Singh, M. V. Kulkarni, S. P. Gokhale, S. H. Chikkali and C. V. Kulkarni, Enhancing the hydrogen storage capacity of Pd-functionalized multi-walled carbon nanotubes, *Appl. Surf. Sci.*, 2012, **258**(8), 3405–3409.
96 N. Karatepe and N. Yuca, Hydrogen adsorption on carbon nanotubes purified by different methods, *Int. J. Hydrogen Energy*, 2011, **36**(17), 11467–11473.
97 A. Kakanakova-Georgieva, I. G. Ivanov, N. Suwannaharn, C.-W. Hsu, I. Cora, B. Pécz, F. Giannazzo, D. G. Sangiovanni and G. K. Gueorguiev, MOCVD of AlN on epitaxial graphene at extreme temperatures, *CrystEngComm*, 2021, **23**(2), 385–390.
98 A. Kakanakova-Georgieva, G. K. Gueorguiev, D. G. Sangiovanni, N. Suwannaharn, I. G. Ivanov, I. Cora, B. Pécz, G. Nicotra and F. Giannazzo, Nanoscale phenomena ruling deposition and intercalation of AlN at the graphene/SiC interface, *Nanoscale*, 2020, **12**(37), 19470–19476.
99 T. G. Mihopoulos, V. Gupta and K. F. Jensen, A reaction-transport model for AlGaN MOVPE growth, *J. Cryst. Growth*, 1998, **195**(1–4), 733–739.
100 R. B. Dos Santos, R. Rivelino, F. de Brito Mota, A. Kakanakova-Georgieva and G. K. Gueorguiev, Feasibility of novel (H 3 C) n X (SiH 3) 3− n compounds (X= B, Al, Ga, In): structure, stability, reactivity, and Raman characterization from *ab initio* calculations, *Dalton Trans.*, 2015, **44**(7), 3356–3366.
101 F. Giannazzo, G. Fisichella, G. Greco, P. Fiorenza and F. Roccaforte, Conductive Atomic Force Microscopy of Two-Dimensional Electron Systems: From AlGaN/GaN Heterostructures to Graphene and MoS2, *Conductive Atomic Force Microscopy: Applications in Nanomaterials*, 2017, pp. 163–185.
102 G. Rajasekaran, R. Kumar and A. Parashar, Tersoff potential with improved accuracy for simulating graphene in molecular dynamics environment, *Mater. Res. Express*, 2016, **3**(3), 035011.
103 H. Wu, D. Wexler, A. R. Ranjbartoreh, H. Liu and G. Wang, Chemical processing of double-walled carbon nanotubes for enhanced hydrogen storage, *Int. J. Hydrogen Energy*, 2010, **35**(12), 6345–6349.
104 V. Gayathri and R. Geetha, Hydrogen adsorption in defected carbon nanotubes, *Adsorption*, 2007, **13**, 53–59.
105 R. Saadi, Z. Saadi, R. Fazaeli and N. E. Fard, Monolayer and multilayer adsorption isotherm models for sorption from aqueous media, *Korean J. Chem. Eng.*, 2015, **32**, 787–799.
106 I. Langmuir, The constitution and fundamental properties of solids and liquids. Part I. Solids, *J. Am. Chem. Soc.*, 1916, **38**(11), 2221–2295.
107 W. Jianlong, Z. Xinmin, D. Decai and Z. Ding, Bioadsorption of lead (II) from aqueous solution by fungal biomass of Aspergillus niger, *J. Biotechnol.*, 2001, **87**(3), 273–277.
108 G. Garcıa, A. Faz and M. Cunha, Performance of Piptatherum miliaceum (Smilo grass) in edaphic Pb and Zn phytoremediation over a short growth period, *Int. Biodeterior. Biodegrad.*, 2004, **54**(2–3), 245–250.
109 J. Zeldowitsch, Adsorption site energy distribution, *Acta Physicochim. URSS*, 1934, **1**(1), 961–973.
110 H. Freundlich, Over the adsorption in solution, *J. Phys. Chem.*, 1906, **57**(385471), 1100–1107.
111 A. L. Myers and J. M. Prausnitz, Thermodynamics of mixed-gas adsorption, *AIChE J.*, 1965, **11**(1), 121–127.
112 B. Van der Bruggen, *Membrane Technology, Kirk-Othmer Encyclopedia of Chemical Technology*, 2017.
113 M. F. Hasan, E. L. First and C. A. Floudas, Cost-effective CO 2 capture based on *in silico* screening of zeolites and process optimization, *Phys. Chem. Chem. Phys.*, 2013, **15**(40), 17601–17618.
114 L. Huang, L. Zhang, Q. Shao, L. Lu, X. Lu, S. Jiang and W. Shen, Simulations of binary mixture adsorption of carbon dioxide and methane in carbon nanotubes: temperature, pressure, and pore size effects, *J. Phys. Chem. C*, 2007, **111**(32), 11912–11920.
115 C. Gu, G.-H. Gao, Y.-X. Yu and T. Nitta, Simulation for separation of hydrogen and carbon monoxide by adsorption on single-walled carbon nanotubes, *Fluid Phase Equilib.*, 2002, **194**, 297–307.
116 X. Huang, H. Yao and Z. Cheng, Hydrogen separation membranes of polymeric materials, *Nanostructured Materials for Next-Generation Energy Storage and Conversion: Hydrogen Production, Storage, and Utilization*, 2017, pp. 85–116.
117 S. Balilehvand, S. M. Hashemianzadeh, S. Razavi and H. Karimi, Investigation of hydrogen and methane adsorption/separation on silicon nanotubes: a hierarchical multiscale method from quantum

mechanics to molecular simulation, *Adsorption*, 2012, **18**(1), 13–22.

118 H. Zhang, Q. Fu, H. Qin, X. Chen, Q. Zhang, Z. Dong, H. Li, S. Wang and M. Wang, An investigation for H_2/N2 adsorptive separation in SIFSIX-2-Cu-i, *Int. J. Hydrogen Energy*, 2023, **48**(67), 26251–26259.

119 S. Yousef, S. Tuckute, A. Tonkonogovas, A. Stankevičius and A. Mohamed, Ultra-permeable CNTs/PES membranes with a very low CNTs content and high H_2/N2 and CH4/N2 selectivity for clean energy extraction applications, *J. Mater. Res. Technol.*, 2021, **15**, 5114–5127.